

Propagation of a Short Intense Laser Pulse in a Curved Plasma Channel

Albert Reitsma and Dino Jaroszynski

Abstract—In this paper, the propagation of a short intense laser pulse in a curved plasma channel is considered. The effects of the shape of the plasma density profile and feedback from the wakefield on the pulse envelope dynamics are studied, with particular attention being paid to the conditions for avoiding laser spot size and centroid oscillations. A possible application to laser wakefield acceleration in the nonlinear regime is discussed.

Index Terms—Laser–plasma interaction, plasma-based acceleration methods, plasma waveguides.

I. INTRODUCTION

LASER wakefield acceleration [1] is one of the several schemes [2] that take advantage of the large-amplitude electric fields of relativistic plasma waves to accelerate electrons. In several recent breakthrough experiments [3]–[5], high-quality electron beams with energies up to 1 GeV have been obtained from the interaction of intense laser pulses with gas jets and preformed plasma channels. The highest energies have been obtained in experiments with preformed plasma channels [6], which extend the laser–plasma interaction distance beyond the Rayleigh length by acting as a waveguide for the laser light. This property makes plasma channels a suitable medium for other various applications as well, for example, X-ray lasing [7], harmonic generation [8], Raman amplification [9], or the emission of betatron radiation [10].

The principle behind plasma channel guiding [11], [12] is that a plasma column with an on-axis density depression acts as a lens for focusing laser light. If there is a perfect balance between the inward bending of light rays through the refractive index gradient and the outward expansion through geometric diffraction, the laser pulse can propagate without spot size or centroid oscillations. This is known as *matched* propagation, which usually requires that the pulse be injected on-axis with the correct spot size, and propagating in the direction of the channel. Sizeable spot size and/or centroid oscillations can occur if the pulse is injected either off-axis, with a nonmatched spot size, or under an angle with the channel axis. This is called *mismatched* propagation: In severe cases, strong laser pulse deformation or loss of intensity due to radiation leaking out of the channel may occur. Plasma channel guiding is not the only way to achieve a long laser–plasma interaction length: Alternative methods include capillary guiding [13] (which relies on total

internal reflection on the boundary of a capillary), relativistic self-focusing [14]–[16], and laser pulse shaping [17].

As with other types of waveguides, such as optical fibers, it is possible with a plasma channel to guide the light along a curved path by bending the waveguide. Light bending in a plasma waveguide has been demonstrated experimentally more than ten years ago for laser pulses with intensities below $10^{17} \text{ W} \cdot \text{cm}^{-2}$, as reported in [18]. In the same publication, analytical and numerical work on spot size and centroid oscillations was presented. It was found that the radial equilibrium position of the laser pulse centroid is displaced from the channel axis, and an estimate for the minimum radius of curvature for radial confinement of the laser pulse in a curved channel was presented. In a recent paper [19], which offers a more in-depth analysis of the matching conditions, off-axis injection is proposed as a way of avoiding centroid oscillations. In the same paper, the effects of self-focusing and wakefields on the propagation of the laser pulse, which become relevant only at laser intensities above $10^{17} \text{ W} \cdot \text{cm}^{-2}$, are studied. Self-focusing is found to be the mechanism that prevents the radial confinement of ultrahigh-intensity laser pulses in a curved channel, whereas the longitudinal pulse evolution in a linear wakefield is found to be very similar to the corresponding evolution in a straight channel [20].

In this paper, we consider laser–plasma interaction in curved channels at still higher intensities (around $10^{18} \text{ W} \cdot \text{cm}^{-2}$), having in mind a possible application to laser wakefield acceleration. We examine in detail the mutual interaction between the laser pulse and the wakefield, leaving the electron acceleration dynamics for possible future investigation. The interest in curved channels for laser wakefield acceleration is that the possibility to bend the laser pulse and/or electron bunch adds some flexibility in beam transport, which might be useful, e.g., in multistage designs.

The reason for increasing the intensity is twofold: We expect that not only the energy gain increases with increasing laser intensity but also the efficiency of the acceleration process. This is because the acceleration (energy transfer from plasma wave to electron) is limited by dephasing [21], i.e., the slippage of electrons from the accelerating region of the wakefield into the decelerating region, which is caused by the fact that the accelerated electrons inside the plasma propagate faster, essentially at c , than the laser pulse, which travels at a group velocity less than c . The energy transfer between the laser pulse and the plasma wave is determined by their mutual feedback, which is known to lead to an explosive instability [22], characterized by a timescale that decreases with increasing laser pulse amplitude. At an intensity around $10^{17} \text{ W} \cdot \text{cm}^{-2}$, the timescale

Manuscript received November 14, 2007. This work was supported by EPSRC [32].

The authors are with the Department of Physics, University of Strathclyde, G4 0NG Glasgow, U.K.

Digital Object Identifier 10.1109/TPS.2008.927148

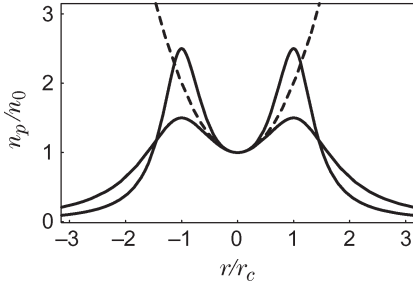


Fig. 1. Channel profile. Solid curves are plots of strong and weak channels (see text for the definition). Dashed curve is the parabolic approximation that is valid for r close to zero.

of the instability is much longer than the dephasing timescale, which results in very little transfer of energy between the laser pulse and the plasma wave during electron acceleration. For intensities of $10^{18} \text{ W} \cdot \text{cm}^{-2}$, both timescales become comparable [23], resulting in significant energy transfer between the laser pulse and the plasma wave, and possibly in a more efficient acceleration of electrons. A complicating factor is that, at higher laser intensities, the instability leads to strong pulse envelope deformation, which in turn affects the stability of the accelerating wakefield on the dephasing timescale.

This paper is organized as follows. In Section II, we introduce a slowly varying envelope equation for the laser pulse envelope dynamics and a quasi-static fluid model for the plasma response (laser wakefield), which form the basis for all numerical simulation results presented here. We review known results for the propagation of short intense laser pulses in plasma, using the 1-D approximation in Section III and considering pulse propagation in a straight channel in Section IV. New results for pulse propagation in curved channels are presented in Section V. Finally, Section VI is devoted to a summary and discussion.

II. ENVELOPE AND WAKEFIELD EQUATIONS

Before presenting the coupled equations for the laser pulse and the wakefield, we find it convenient to introduce the following notation. We define a radial coordinate $r = (x^2 + z^2)^{1/2} - R$ such that $r = 0$ corresponds to a circle or circle segment in the (x, z) plane with radius R , which is the shape of our curved plasma channel. The angle ϕ is defined in the usual way as $\phi = \arctan(x/z)$. To simplify the problem, we adopt a 2-D geometry by dropping all y -dependences from the equations. The equilibrium plasma density n_p is assumed to be parabolic close to $r = 0$: $n_p(r) = n_0(1 + r^2/r_c^2)$ for $r \ll r_c$, where $r_c \ll R$ determines the curvature of the density profile. For the actual density profile used in the simulations, we take two different forms, as shown in Fig. 1. In the limit of large r , the density of both profiles is seen to approach zero, whereas a maximum is observed at $r = r_c$. The reasons for choosing this type of profile are the following: 1) It is close to experimentally observed radial density distributions [24], [25], and 2) a parabolic profile does not allow us to model radiation leakage from the channel due to the unrealistic limit of infinite density at large r . The upper curve, which we shall refer to as

a *strong* channel, has a profile that rises steeper than parabolic for $|r| < r_c$, whereas the lower curve, which we refer to as a *weak* channel, has a profile that rises less steep than parabolic for $|r| < r_c$. Not surprisingly, our simulation results show that a strong channel is better at preventing radiation leakage than a weak channel.

With the usual definition of a as the complex envelope of the laser potential in dimensionless form, the slowly varying envelope equation in a curved channel becomes

$$2 \left(i\omega_0 + c \frac{\partial}{\partial s} \right) \left(\frac{\partial a}{\partial t} - i\omega_0 \frac{r}{R} a \right) + c^2 \frac{\partial^2 a}{\partial r^2} - \Omega_p^2 a = 0.$$

In the aforementioned equation, ω_0 denotes the laser carrier frequency, $s = R\phi - ct$ is the comoving coordinate, and $\Omega_p(r, s, t)$ is a *local*, i.e., space- and time-varying, plasma frequency. It is defined by $\Omega_p^2 = 4\pi n e^2 / m\gamma$, where n is the density and γ is the Lorentz factor of plasma electrons. The derivation of the envelope equation can be found in [19]. We only note one additional approximation $(i\omega_0 + c\partial_s)^2 a \approx i\omega_0(i\omega_0 + c\partial_s)a$ that has been made here in order to speed up the numerical algorithm for solving the envelope equation. We have checked that this can be done without changing the outcome significantly.

The calculation of the local plasma frequency is done with the following quasi-static fluid equation for the plasma response

$$\left(1 - \frac{\partial}{\partial r} \left[\frac{1}{k_p^2} \frac{\partial}{\partial r} \right] \right) \frac{\partial^2 \psi}{\partial s^2} = \frac{k_p^2}{2} \left(\frac{1 + |a|^2/2}{[1 + \psi]^2} - 1 \right) + \frac{\partial^2}{\partial r^2} \left(\psi - \frac{|a|^2}{4} \right)$$

where ψ denotes the dimensionless wakefield potential and $k_p^2(r) = 4\pi n_p(r)e^2/mc^2$. This equation is basically the one given in [26] and becomes exact in the 1-D nonlinear limit and the 2-D linear limit. Note that we use the wakefield equation corresponding to a straight channel, which can be justified if the curvature is negligible for an arc length of several plasma wavelengths. Indeed, for linear wakefields, it can be shown [19] that the additional terms are smaller by an order of at least r/R . In terms of the wakefield potential, the local plasma frequency is given by

$$\frac{\Omega_p^2}{c^2} = \frac{k_p^2}{1 + \psi} + \frac{\partial^2 \psi}{\partial r^2}$$

where a slight difference with the result of [26] is observed. Our formula for Ω_p^2 is consistent with energy conservation, where the wakefield energy density is given by

$$\frac{c^2}{2} \left(\left[\frac{\partial \psi}{\partial s} \right]^2 + \left[\frac{\partial \psi}{\partial r} \right]^2 + \frac{1}{k_p^2} \left[\frac{\partial^2 \psi}{\partial r \partial s} \right]^2 + k_p^2 \frac{\psi^2}{1 + \psi} \right)$$

and the laser pulse energy density by

$$|i\omega_0 a + c\partial a/\partial s|^2$$

in units consistent with our dimensionless notation.

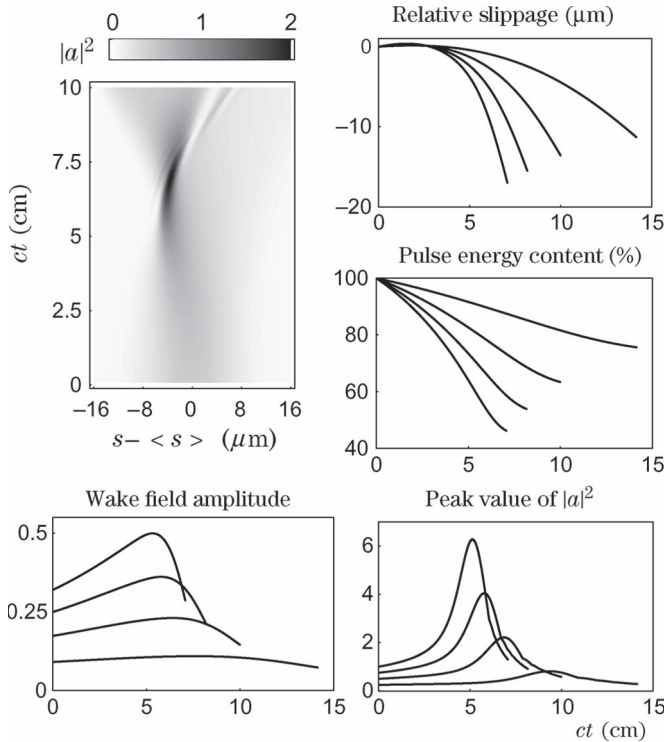


Fig. 2. One-dimensional simulation results. Contour plot of $|a|^2$ for $a_0^2 = 0.5$. Graphs of relative slippage $\langle s \rangle + (c - v_g)t$, laser pulse energy content, wakefield amplitude (dimensionless), and peak value of $|a|^2$ for $a_0^2 = 0.25, 0.5, 0.75$, and 1 . The curves can be distinguished by the duration of the simulation, where a longer duration corresponds to a lower initial amplitude.

III. 1-D APPROXIMATION

For the 1-D simulations, we choose an initially Gaussian pulse

$$a(s) = a_0 \exp(-s^2/2s_l^2)$$

where a_0 denotes the dimensionless amplitude of the laser pulse and $s_l = 7.5 \mu\text{m}$ is the laser pulse length. With this choice of pulse length, we get near-resonant excitation of the wakefield in a plasma with our chosen density $n_0 = 10^{18} \text{ cm}^{-3}$. At this density, the linear group velocity $v_g = c(1 - 1/\gamma_g^2)^{1/2}$, which corresponds to a Lorentz factor $\gamma_g = (n_{cr}/n_0)^{1/2} \approx 42$, is determined from the critical density $n_{cr} = m\omega_0^2/4\pi e^2$, assuming a laser wavelength of 800 nm.

The 1-D simulation results are shown in Fig. 2, where the contour plot shows $|a|^2$ as a function of s and t for $a_0^2 = 0.5$, corresponding to a peak intensity of about $10^{18} \text{ W} \cdot \text{cm}^{-2}$. We see an increase of the pulse amplitude accompanied by strong pulse compression, with a very narrow peak being observed around $ct \approx 7 \text{ cm}$, followed by pulse spreading and envelope modulation. These features are typical of the explosive feedback instability described in Section I. Note that, for reasons of convenience only, the s -coordinate is given relative to its average value

$$\langle s \rangle = \frac{\int s|a|^2 ds}{\int |a|^2 ds}$$

which means that phase slippage effects cannot be easily read from the contour plot. Instead, one should look at the graph of $\langle s \rangle + (c - v_g)t$ versus ct to get a feel for this. This graph shows the difference in average s -coordinate between the actual simulation result and a rigid pulse propagating continually at the linear group velocity v_g , with four choices of laser pulse amplitude $a_0^2 = 0.25, 0.5, 0.75$, and 1 . It is observed that, initially, the simulated laser pulses move, on average, slightly faster than the rigid pulse, while later on, they propagate much slower, and this effect becomes more pronounced with increasing pulse amplitude.

This observation can be explained as follows. According to photon kinetic theory [27], [28], it is possible to view the pulse as a collection of photons with different group velocities $c(1 - \Omega_p^2/\Omega^2)^{1/2}$, where the photon frequency Ω is given by a local dispersion relation $\Omega^2 = c^2k^2 + \Omega_p^2(s, t)$, and k is the photon wavenumber. At early times, when all photons have frequencies close to ω_0 , the slippage is determined mostly by the local plasma frequency. Photons at the head of the pulse, where $\Omega_p^2 \approx 4\pi n_0 e^2/m$, are seen to propagate at v_g , whereas photons toward the back of the pulse, where Ω_p^2 decreases due to the presence of the wake, are seen to propagate slightly faster. Thus, the pulse is compressed, and its average velocity is higher than v_g . At later times, the decrease of Ω due to photon deceleration (i.e., adiabatic frequency redshift in the time-varying medium) is the dominant effect, and the pulse slows down as it loses energy to the wakefield. The energy loss is greater at higher pulse amplitude, as seen in the graph of pulse energy content versus ct , which explains why the slowdown is more dramatic at higher a_0 .

The last two graphs shown in Fig. 2 contain the dimensionless wakefield amplitude and the peak value of $|a|^2$ as functions of ct . We note here that the evolution is seen to be similar in all four cases, but happens on different timescales, in accordance with the scaling of the explosive feedback instability. The simulations end at different times t_f such that $a_0 t_f$ has a constant value [29]. For comparison, dephasing in a wakefield propagating continually at the linear group velocity v_g takes place at $ct \approx 5.8 \text{ cm}$: At this propagation distance, there is a clear difference between the simulation results for $a_0^2 = 1/4$ and $a_0^2 = 1$, with the latter showing much more energy transfer between laser pulse and plasma wave.

IV. STRAIGHT CHANNEL

To develop a convenient “mental picture” for the transverse dynamics, we first neglect the effects of finite pulse length and channel curvature. This reduces the envelope equation to

$$2i\omega_0 \frac{\partial a}{\partial t} + c^2 \frac{\partial^2 a}{\partial r^2} - \Omega_p^2 a = 0$$

which has the form of a Schrodinger equation, where the diffraction term plays the role of the kinetic energy, and Ω_p^2 plays the role of the potential. For example, it is well known that a parabolic plasma channel

$$\Omega_p^2 = \frac{4\pi e^2 n_0}{m} \left(1 + \frac{r^2}{r_c^2} \right)$$

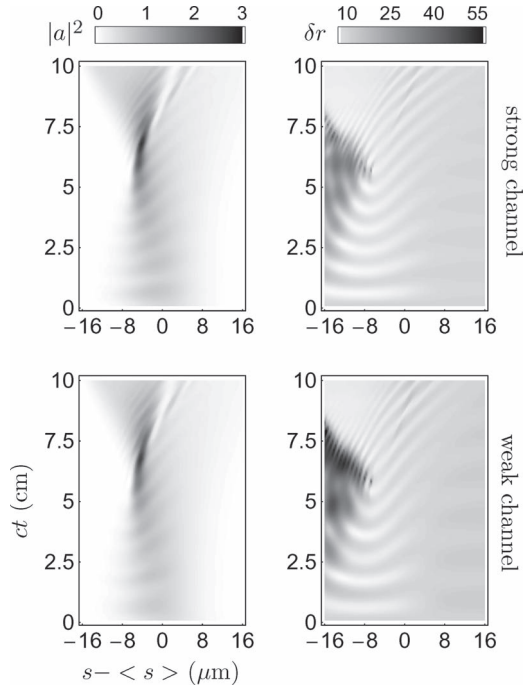


Fig. 3. Simulation results for strong and weak straight channels. Contour plots of envelope $|a|^2$ (lineout at $r = 0$) and slice width δr as functions of s and t .

is equivalent to the quantum harmonic oscillator, and its Hermite–Gaussian eigenfunctions are seen to correspond to the laser modes of the plasma channel. This gives us another interpretation of the matching conditions: Matched propagation occurs if the initial laser distribution is equal to one of the modes of the channel (often the lowest order mode in practice), and mismatch occurs for multimode propagation, where centroid or spot size oscillations are the result of beating of several laser modes.

To describe the effect of finite pulse length, a representation of the laser distribution in terms of s -slices is useful. Each slice can undergo spot size and/or centroid oscillations if there is a mismatch between the slice distribution and the potential at the slice location (remember that Ω_p^2 now varies with s as well as with r). The slice oscillations are not independent, as the shape of the potential at a given slice is determined by the wakefield excited by all slices in front of it. Under certain conditions, this feedback between the slice oscillations and the wakefield dynamics can lead to instabilities [30].

We now discuss numerical examples of laser pulse propagation in a straight channel, as shown in Fig. 3. For this simulation, the channel parameters are $n_0 = 10^{18} \text{ cm}^{-3}$ as before, and $r_c = 125 \text{ } \mu\text{m}$. The initial laser profile is double Gaussian

$$a(r, s) = a_0 \exp\left(-[r - r_0]^2/2r_l^2 - s^2/2s_l^2\right)$$

where a_0 is the pulse amplitude, r_0 is the laser offset relative to the channel axis, r_l is the spot size, and s_l is the pulse length. We choose $a_0^2 = 0.5$, $r_0 = 0$, corresponding to on-axis injection, $r_l = 25 \text{ } \mu\text{m}$, which gives matched propagation in a parabolic channel, and $s_l = 7.5 \text{ } \mu\text{m}$ as before. Fig. 3 contains contour plots of $|a|^2$ evaluated at $r = 0$ and the slice width δr

as a function of s and t . As before, s is given relative to its average value

$$\langle s \rangle = \frac{\int s |a|^2 dr ds}{\int |a|^2 dr ds}.$$

The slice width δr is defined by

$$[\delta r]^2 = \frac{\int (r - \langle r \rangle[s])^2 |a|^2 dr}{\int |a|^2 dr}$$

where $\langle r \rangle[s]$ is a local average of r

$$\langle r \rangle[s] = \frac{\int r |a|^2 dr}{\int |a|^2 dr}.$$

For on-axis injection in a straight channel, symmetry dictates that $\langle r \rangle[s] = 0$, i.e., there are no centroid oscillations in all slices.

As all slices are initially matched to the parabolic channel profile, spot-size oscillations in the very first slices of the laser pulse, i.e., in a region where wakefield effects are negligible, are due to the difference in matching conditions between the parabolic channel and the nonparabolic profiles used in the simulation (as shown in Fig. 1). Although it is hard to distinguish in the contour plots on the right-hand side of Fig. 3, the first slices actually undergo slight spot-size oscillations: Compared with the parabolic channel, the matched spot size for the strong (weak) channel is slightly smaller (larger).

Much easier to observe are the spot-size oscillations of slices further back in the laser pulse, for which the difference in matching conditions is even greater (parabolic versus nonparabolic profiles plus wakefield excited by preceding slices). For $ct \leq 5 \text{ cm}$, we observe that the equilibrium spot size, as well as the period of oscillation, is largest for slices at the front of the pulse, and they go through a minimum value toward the back of the pulse. As expected, whenever a slice is contracted, a corresponding increase in the on-axis value of $|a|^2$ is observed in the contour plots on the left-hand side of Fig. 3. Apart from these additional ripples due to the coupling between longitudinal and transverse pulse dynamics, the contour plots of $|a|^2$ show exactly the same features as the 1-D plot shown in Fig. 2: pulse compression and amplitude increase, followed by pulse spreading and envelope modulation. We have also looked at the energy transfer from the laser pulse to the wakefield, which is slightly less efficient compared with the 1-D case, and the phase slippage behavior, which is similar (simulation results not shown here). After the time of maximum longitudinal compression ($ct \approx 7 \text{ cm}$), the transverse dynamics changes dramatically, and we see that the spot-size oscillations damp out, while their period decreases.

V. CURVED CHANNEL

As stated in Section I, the main effect of the channel curvature is to shift the radial equilibrium position r_{eq} of the laser pulse away from the channel axis. Physically, r_{eq} is determined by the balance between the refractive index gradient that bends the light rays inward and the centrifugal force that pulls them

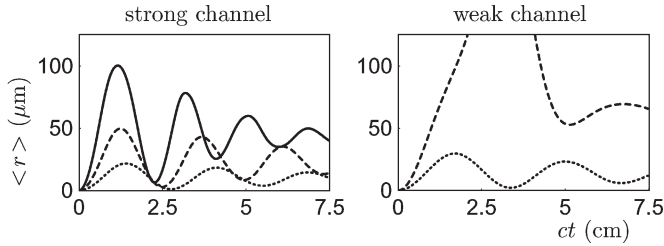


Fig. 4. Simulation results for on-axis injection in a curved channel. Graphs of laser pulse centroid evolution, with solid line corresponding to $R = 30$ cm and dashed and dotted lines to $R = 75$ and 200 cm, respectively.

out of the channel. Mathematically, this is formulated with the help of an effective potential

$$\Omega_{\text{eff}}^2 = \Omega_p^2 - 2\omega_0^2 \frac{r}{R}$$

or, equivalently, an effective plasma density

$$n_{\text{eff}} = \frac{n}{\gamma} - 2n_{cr} \frac{r}{R}$$

and the requirement that $\partial\Omega_{\text{eff}}^2/\partial r = 0$, i.e., the absence of a force. From the aforementioned condition, one can derive the minimum value of R required for radial confinement of the laser pulse. In our simulations, we have used three values for R : 1) a large value ($R = 200$ cm); 2) an intermediate value ($R = 75$ cm); and 3) a small value ($R = 30$ cm). It turns out that, for $R = 30$ cm, only the strong channel is able to confine the laser pulse. Thus, for this value of R , we have not simulated propagation in the weak channel.

As expected, we observe that laser pulses injected on the channel axis undergo centroid oscillations of relatively large amplitude. This is shown in Fig. 4, which shows the graphs of the average radial position

$$\langle r \rangle = \frac{\int r |a|^2 dr ds}{\int |a|^2 dr ds}$$

as a function of t for $a_0^2 = 0.5$ and different values of R , with all other simulation parameters being the same as for the straight-channel simulations.

Four other interesting observations in Fig. 4 are the following: 1) a general damping of the oscillation amplitude; 2) a variation of the oscillation period with R ; 3) an overall drift of the centroid toward smaller r ; and 4) for the $R = 75$ -cm case in the weak channel, an increase of $\langle r \rangle$ above r_c at $ct \approx 2$ cm, followed by a decrease below r_c at $ct \approx 4$ cm, as if the laser pulse exits and reenters the channel.

To begin with the last point, as exit and reentry of the whole laser pulse are clearly impossible, there must be another explanation for this observation. What happens is that, although a large part of the pulse is indeed lost from the channel, a small part (corresponding to a 30% energy fraction of the initial laser pulse) remains inside. The oscillation of this 30% shows up at $ct > 4$ cm, when the other 70% has left the simulation box. What is not clearly visible is that two occasions of pulse loss from the channel occur for the $R = 30$ cm case in the strong

channel simulation, corresponding to 20% and 8% of the initial laser pulse energy.

The overall centroid drift toward smaller r can be understood as an effect of the curvature of the wakefield wavefronts, a feature that is common to wakefields excited in plasma channels [31]. Just as wakefield excitation causes a slice-to-slice variation in the matching conditions of the spot size, it is also responsible for slice-to-slice variations in the matching conditions of the centroid. In other words, the s -dependence of Ω_p^2 causes r_{eq} to be s dependent as well. It turns out that the curvature always causes r_{eq} to decrease with decreasing s , i.e., the wake excited by the head of the pulse deflects the tail toward lower r .

The variation of the oscillation period with R is an effect associated with the nonparabolic nature of the density profile used in the simulation. The frequency ω_c of the centroid oscillation is roughly given by

$$\omega_c^2 = \frac{c^2}{\omega_0^2} \frac{\partial^2 \Omega_{\text{eff}}^2}{\partial r^2} \Big|_{r=r_{\text{eq}}}$$

which is independent of r_{eq} (and, therefore, independent of R) for a parabolic Ω_p^2 , but varies with R for a nonparabolic profile. For the strong channel, a decrease in R corresponds to a shorter oscillation period, whereas the weak channel exhibits the opposite trend. Finally, the damping of the centroid oscillation is attributed to the feedback between the laser pulse and the plasma wave.

The simulation results shown in Fig. 5 have been obtained with the same parameters as the ones shown in Fig. 4, except for injection of the pulse around $r_0 = r_{\text{eq}}$, which is the strategy for avoiding centroid oscillations recommended in [19]. We have taken the unperturbed profiles of Fig. 1 for the calculation of r_{eq} (not the parabolic approximation), which gives $r_{\text{eq}} = 53.1, 29.0,$ and $12.9 \mu\text{m}$ at $R = 30, 75,$ and 200 cm for the strong channel and $r_{\text{eq}} = 40.6$ and $13.8 \mu\text{m}$ at $R = 75$ and 200 cm for the weak channel.

In Fig. 5, the four features that are worth noting are the following: 1) a drift of the centroid toward the channel axis; 2) occurrence of pulse centroid oscillations in spite of injection at $r_0 = r_{\text{eq}}$ (despite a much smaller amplitude than those observed in Fig. 4); 3) a decrease of the timescale of pulse energy loss and pulse amplitude evolution with decreasing R ; and 4) a dramatic increase of pulsewidth δr for the $R = 75$ cm weak-channel simulation.

The explanation of the drift toward smaller r is the same as before, namely, a deflection of the laser pulse's tail in the wakefield excited by the head of the pulse. To investigate the cause of the pulse centroid oscillations, we show contour plots of the slice centroid and slice width as functions of s and t for one particular case ($R = 75$ cm in a strong channel) in Fig. 6. In the contour plot on the left-hand side, we observe that *all* slices, even the ones in the head of the pulse where wakefield effects are negligible, undergo centroid oscillations. Evidently, we cannot explain this in terms of deflection of the tail of the laser pulse induced by the wakefield of the head, for in that case, we would observe oscillations in the tail of the pulse only.

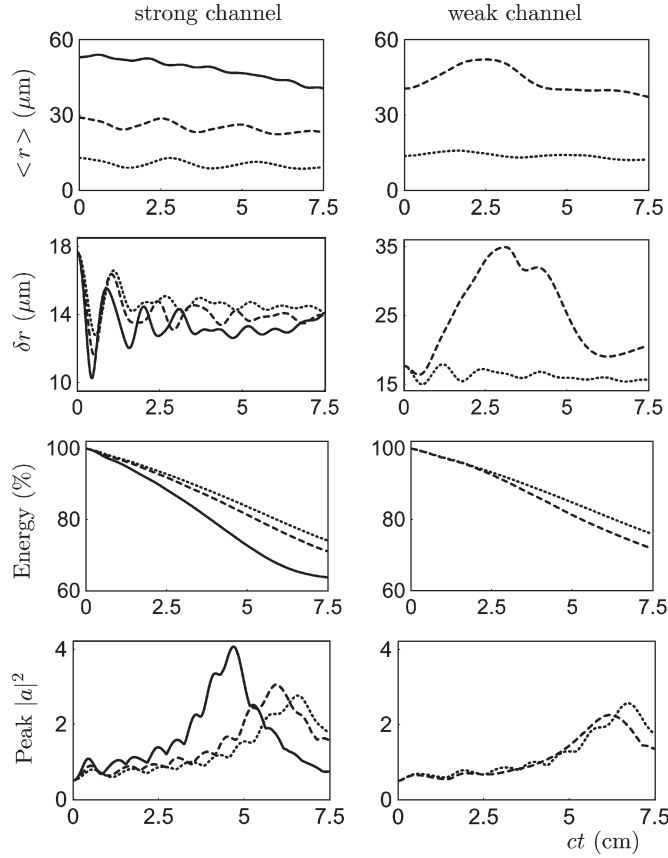


Fig. 5. Simulation results for off-axis injection in a curved channel. (From top to bottom) Graphs of laser pulse centroid, laser pulsewidth, laser pulse energy, and peak value of $|a|^2$. Solid lines correspond to $R = 30$ cm, and dashed and dotted lines correspond to $R = 75$ and 200 cm, respectively.

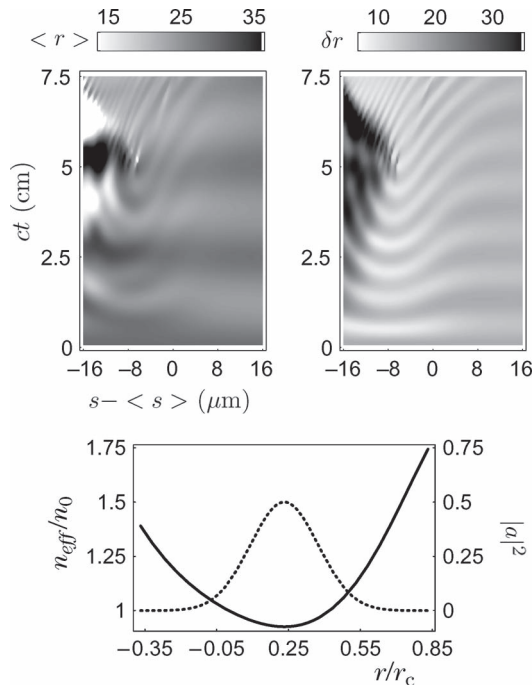


Fig. 6. Simulation results for $R = 75$ cm in a strong channel with off-axis injection. (Top) Contour plots of slice centroid and slice width as functions of s and t . (Bottom) Profiles of effective density and initial laser pulse envelope.

Instead, we offer the following explanation. Consider the graph at the bottom of Fig. 6, which shows the initial laser envelope and the effective density in front of the laser pulse

$$n_{\text{eff}}(r) = n_p(r) - 2n_{\text{cr}} \frac{r}{R}.$$

Remember that the effective density is basically the potential for the radial motion of the laser pulse. Thus, the asymmetry of n_{eff} around $r = r_{\text{eq}}$ in the pulse region gives rise to a net force in the negative r -direction, which provides the initial impulse for the centroid oscillation, and this applies to all slices. Note that, for a weak channel, the initial impulse is in the positive r -direction, as observed in Fig. 5. There is no net force for a perfectly parabolic channel, as, in this case, the effective density

$$n_0 \left(1 - \frac{r_{\text{eq}}^2}{r_c^2} + \left[\frac{r - r_{\text{eq}}}{r_c} \right]^2 \right)$$

is always symmetric around $r = r_{\text{eq}}$. Likewise, the matched spot size at $r = r_{\text{eq}}$ does not vary with R if n_p is parabolic, and it becomes smaller (larger) for decreasing R in a strong (weak) channel. Thus, we expect that an initial spot size of $r_l = 25$ μm , which is matched for on-axis injection in a parabolic profile, is too big for propagation in a strong channel. In addition, indeed, in the contour plot on the right-hand side of Fig. 6, we observe sizeable spot-size oscillations, even at the head of the laser pulse where wakefield effects are negligible. We have checked that it is possible to almost eliminate spot-size and centroid oscillations in this region by choosing slightly smaller (larger) values of r_0 and r_l in a strong (weak) channel.

The decrease in timescale of pulse energy loss and pulse amplitude evolution with decreasing R can be explained by the scaling of pump depletion length $L_d \propto (n_{\text{cr}}/n)^{-3/2}$ with plasma density n [22]. A shorter pump depletion length is found at higher plasma density $n = n_p(r_{\text{eq}})$, which corresponds to a pulse equilibrium position r_{eq} that is farther from the axis, which in turn corresponds to a smaller value of R . In accordance with this are the observations (not shown here) of oscillations in the pulse energy loss rate that occur for on-axis injection: As the pulse moves in radial direction, it encounters regions of different plasma densities, and it couples more efficiently to the wakefield at higher n .

The dramatic increase of δr for the $R = 75$ -cm weak-channel case turns out to be due to pulse loss from the channel. Although the bulk of the pulse remains within the channel, the small fraction that manages to escape (corresponding to 3% of the initial laser pulse energy) has a disproportionate effect on the calculation of δr . Later on, when the escaped radiation has escaped from the simulation box, δr is seen to return to a more “normal” value.

VI. SUMMARY AND DISCUSSION

In this paper, we have presented simulations of short intense laser pulses propagating in underdense plasma based on coupled equations for a slowly varying laser pulse envelope and a quasi-static fluid description for the plasma. In Sections III

and IV, we reviewed several well-known results for pulse propagation in the 1-D approximation and for a straight channel in 2-D geometry. In these sections, we have emphasized those aspects that are most relevant to the new results of intense pulse propagation in a curved channel, which we have presented in Section V.

The 1-D simulations merely confirm that the longitudinal dynamics of short-pulse propagation in a plasma is determined by a well-known explosive feedback instability. The timescale of this instability depends on the laser pulse amplitude, such that pulses of higher intensity couple more efficiently to the wakefield on the timescale of electron dephasing, which is the motivation for extending our investigations from the linear into the nonlinear wakefield regime.

For the presentation of 2-D straight-channel simulation results, we have used a helpful “mental picture” of Ω_p^2 as a potential for the transverse motion of the laser pulse, while the feedback between the laser pulse and the wakefield has been elegantly treated with a subdivision of the laser pulse into s -slices.

For stable propagation in a curved channel, it is important to avoid centroid and spot-size oscillations as much as possible. In principle, the matching conditions are straightforward: injection of the laser pulse around the equilibrium position r_{eq} , which is the minimum of the effective potential $\Omega_{\text{eff}}^2 = \Omega_p^2 - 2\omega_0^2 r/R$. The matching spot size is determined by the value of $\partial^2 \Omega_{\text{eff}}^2 / \partial r^2$ at $r = r_{\text{eq}}$. However, due to the s -dependence of Ω_{eff}^2 , these quantities vary from slice to slice. Furthermore, due to the curvature of the wakefield wavefronts, there is a deflection of the tail of the laser pulse in the wakefield induced by the head, which causes an overall drift of the laser pulse toward the channel axis.

In our simulations, we have used the following two different profiles for the unperturbed plasma density (see Fig. 1): a strong channel with a profile that rises more steeply than the parabolic one and a weak channel with a profile that rises less steeply. While there is not much difference in the simulation results for strong and weak straight channels, we have found considerable differences in the performance of strong and weak curved channels. For a radius of curvature of 30 cm and an on-axis plasma density of 10^{18} cm^{-3} , only the strong channel is able to confine the laser pulse. For a radius of curvature of 75 cm, the weak channel is able to confine the bulk of the radiation only if the laser pulse is injected at the equilibrium position, not for on-axis injection.

Generally, for a strong (weak) channel, the periods of the centroid and spot-size oscillations, as well as the matched spot size, are functions that decrease (increase) with decreasing plasma channel radius of curvature, and they are smaller (larger) than for a parabolic channel. Furthermore, the effective density, which is always symmetric around $r = r_{\text{eq}}$ in a parabolic channel, becomes asymmetric around $r = r_{\text{eq}}$ in a nonparabolic channel. This feature causes centroid oscillations for a laser pulse with an initially symmetric (e.g., Gaussian) profile if the pulse is injected at a radial offset $r_0 = r_{\text{eq}}$, a problem that can be solved by choosing a slightly different value of r_0 . Last, we have found that the radius of curvature of the plasma channel influences the coupling efficiency from

the laser pulse to the wakefield, as it determines the value of r_{eq} and, therefore, the local value of the plasma density, which in turn determines the pump depletion length.

Finally, we comment on the possible application of curved plasma channels to laser wakefield acceleration. The results in this paper demonstrate that, in principle, a short intense laser pulse can be guided in a curved plasma channel with efficient coupling of energy to the wakefield if one carefully observes the conditions for stable propagation, i.e., injection with a radial offset close to the equilibrium position with a matched spot size. The intricate feedback between the laser pulse and the wakefield is responsible for some unavoidable residual spot-size and centroid oscillations, as it is virtually impossible to meet the matching conditions in all slices simultaneously. Equally unavoidable is a drift of the laser pulse toward the channel axis. Although these effects need not be detrimental for the stability of the electron acceleration, one also has to consider the following effects.

As pointed out in [19], due to the dephasing length being much shorter than the circle circumference, only a slight bend can be given to the laser pulse and/or electron bunch in a single acceleration stage. Another important point is the transverse stability of the electron motion. Just as the balance between the refractive index gradient and the centrifugal force keeps the laser pulse inside the channel, a balance between the wakefield transverse force and the centrifugal force is required for the radial confinement of electrons. The magnitude of the required force increases with increasing electron energy, and the associated acceleration gives rise to the emission of synchrotron radiation [10].

Furthermore, one has to consider the stability of a bunch of electrons rather than a single particle. For example, the electrons will almost certainly come out of the channel under an angle with the channel axis. The question is how predictable this angle is and how much it will vary from electron to electron. Furthermore, as different electrons sample different parts of a highly dynamic wakefield (at least in the nonlinear regime), a dramatic increase of energy spread may result. All these issues need to be investigated further in order to assess the feasibility of laser wakefield acceleration in curved plasma channels.

REFERENCES

- [1] T. Tajima and J. M. Dawson, “Laser electron accelerator,” *Phys. Rev. Lett.*, vol. 43, no. 4, pp. 267–270, Jul. 1979.
- [2] E. Esarey, P. Sprangle, J. Krall, and A. Ting, “Overview of plasma-based accelerator concepts,” *IEEE Trans. Plasma Sci.*, vol. 24, no. 2, pp. 252–288, Apr. 1996.
- [3] S. P. D. Mangles, C. D. Murphy, Z. Najmudin, A. G. R. Thomas, J. L. Collier, A. E. Dangor, E. J. Divall, P. S. Foster, J. G. Gallacher, C. J. Hooker, D. A. Jaroszynski, A. J. Langley, W. B. Mori, P. A. Norreys, F. S. Tsung, R. Viskup, B. R. Walton, and K. Krushelnick, “Monoenergetic beams of relativistic electrons from intense laser–plasma interactions,” *Nature (London)*, vol. 431, no. 7008, pp. 535–538, Sep. 2004.
- [4] C. G. R. Geddes, C. Toth, J. van Tilborg, E. Esarey, C. B. Schroeder, D. Bruhwiler, C. Nieter, J. Cary, and W. P. Leemans, “High-quality electron beams from a laser wakefield accelerator using plasma-channel guiding,” *Nature (London)*, vol. 431, no. 7008, pp. 538–541, Sep. 2004.
- [5] J. Faure, Y. Glinec, A. Pukhov, S. Kiselev, S. Gordienko, E. Lefebvre, J.-P. Rousseau, F. Burgy, and V. Malka, “A laser–plasma accelerator producing monoenergetic electron beams,” *Nature (London)*, vol. 431, no. 7008, pp. 541–544, Sep. 2004.

- [6] W. P. Leemans, B. Nagler, A. J. Gonsalves, C. Tóth, K. Nakamura, C. G. R. Geddes, E. Esarey, C. B. Schroeder, and S. M. Hooker, "GeV electron beams from a centimetre-scale accelerator," *Nature Phys.*, vol. 2, no. 10, pp. 696–699, Oct. 2006.
- [7] J. J. Rocca, V. Shlyaptsev, F. G. Tomasel, O. D. Cortázar, D. Hartshorn, and J. L. A. Chilla, "Demonstration of a discharge pumped table-top soft-X-ray laser," *Phys. Rev. Lett.*, vol. 73, no. 16, pp. 2192–2195, Oct. 1994.
- [8] A. Rundquist, C. G. Durfee, III, Z. Chang, C. Herne, S. Backus, M. M. Murnane, and H. C. Kapteyn, "Phase-matched generation of coherent soft X-rays," *Science*, vol. 280, no. 5368, pp. 1412–1415, May 1998.
- [9] Y. Ping, I. Geltner, A. Morozov, N. J. Fisch, and S. Suckewer, "Raman amplification of ultrashort laser pulses in microcapillary plasmas," *Phys. Rev. E, Stat. Phys. Plasmas Fluids Relat. Interdiscip. Top.*, vol. 66, no. 4, p. 046 401, Oct. 2002.
- [10] D. A. Jaroszynski, R. Bingham, E. Brunetti, B. Ersfeld, J. Gallacher, B. van der Geer, R. Issac, S. P. Jamison, D. Jones, M. de Loos, A. Lyachev, V. Pavlov, A. Reitsma, Y. Saveliev, G. Vieux, and S. M. Wiggins, "Radiation sources based on laser–plasma interactions," *Philos. Trans. Roy. Soc. London A, Math. Phys. Sci.*, vol. 364, no. 1840, pp. 689–710, Mar. 2006.
- [11] P. Sprangle, E. Esarey, J. Krall, and G. Joyce, "Propagation and guiding of intense laser pulses in plasmas," *Phys. Rev. Lett.*, vol. 69, no. 15, pp. 2200–2203, Oct. 1992.
- [12] D. Spence and S. Hooker, "Investigation of a hydrogen plasma waveguide," *Phys. Rev. E, Stat. Phys. Plasmas Fluids Relat. Interdiscip. Top.*, vol. 63, no. 1, p. 015 401, Jan. 2001.
- [13] C. Courtois, A. Couairon, B. Cros, J. R. Marquès, and G. Matthieussent, "Propagation of intense ultrashort laser pulses in a plasma filled capillary tube: Simulations and experiments," *Phys. Plasmas*, vol. 8, no. 7, pp. 3445–3456, Jul. 2001.
- [14] G.-Z. Sun, E. Ott, Y. C. Lee, and P. Guzdar, "Self-focusing of short intense pulses in plasmas," *Phys. Fluids*, vol. 30, no. 2, pp. 526–532, Feb. 1987.
- [15] T. Kurki-Suonio, P. J. Morrison, and T. Tajima, "Self-focusing of an optical beam in a plasma," *Phys. Rev. A, Gen. Phys.*, vol. 40, no. 6, pp. 3230–3239, Sep. 1989.
- [16] B. Hafizi, A. Ting, P. Sprangle, and R. F. Hubbard, "Relativistic focusing and ponderomotive channeling of intense laser beams," *Phys. Rev. E, Stat. Phys. Plasmas Fluids Relat. Interdiscip. Top.*, vol. 62, no. 3, pp. 4120–4125, Sep. 2000.
- [17] E. Esarey, P. Sprangle, J. Krall, A. Ting, and G. Joyce, "Optically guided laser wake-field acceleration," *Phys. Fluids, B Plasma Phys.*, vol. 5, no. 7, pp. 2690–2697, Jul. 1993.
- [18] Y. Ehrlich, C. Cohen, A. Zigler, J. Krall, P. Sprangle, and E. Esarey, "Guiding of high intensity laser pulses in straight and curved plasma channel experiments," *Phys. Rev. Lett.*, vol. 77, no. 20, pp. 4186–4189, Nov. 1996.
- [19] A. J. W. Reitsma and D. A. Jaroszynski, "Propagation of a weakly nonlinear laser pulse in a curved plasma channel," *Phys. Plasmas*, vol. 14, no. 5, p. 053 104, May 2007.
- [20] D. F. Gordon, B. Hafizi, R. F. Hubbard, J. R. Peñano, P. Sprangle, and A. Ting, "Asymmetric self-phase modulation and compression of short laser pulses in plasma channels," *Phys. Rev. Lett.*, vol. 90, no. 21, p. 215 001, May 2003.
- [21] R. F. Hubbard, P. Sprangle, and B. Hafizi, "Scaling of accelerating gradients and dephasing effects in channel-guided laser wakefield accelerators," *IEEE Trans. Plasma Sci.*, vol. 28, no. 4, pp. 1159–1169, Aug. 2000.
- [22] S. V. Bulanov, I. N. Inovenkov, V. I. Kirsanov, N. M. Naumova, and A. S. Sakharov, "Nonlinear depletion of ultrashort and relativistically strong laser pulses in an underdense plasma," *Phys. Fluids, B Plasma Phys.*, vol. 4, no. 7, pp. 1935–1942, Jul. 1992.
- [23] A. J. W. Reitsma, R. A. Cairns, R. Bingham, and D. A. Jaroszynski, "Efficiency and energy spread in laser-wakefield acceleration," *Phys. Rev. Lett.*, vol. 94, no. 8, p. 085 004, Mar. 2005.
- [24] N. A. Bobrova, A. A. Esaulov, J.-I. Sakai, P. V. Sasorov, D. J. Spence, A. Butler, S. M. Hooker, and S. V. Bulanov, "Simulations of a hydrogen-filled capillary discharge waveguide," *Phys. Rev. E, Stat. Phys. Plasmas Fluids Relat. Interdiscip. Top.*, vol. 65, no. 1, p. 016 407, Jan. 2002.
- [25] B. H. P. Broks, K. Garloff, and J. J. A. M. van der Mullen, "Nonlocal–thermal–equilibrium model of a pulsed capillary discharge waveguide," *Phys. Rev. E, Stat. Phys. Plasmas Fluids Relat. Interdiscip. Top.*, vol. 71, no. 1, p. 016 401, Jan. 2005.
- [26] N. E. Andreev, S. V. Kuznetsov, A. A. Pogosova, L. C. Steinhauer, and W. D. Kimura, "Modeling of laser wakefield acceleration at CO₂ laser wavelengths," *Phys. Rev. Spec. Top., Accel. Beams*, vol. 6, no. 4, p. 041 301, Apr. 2003.
- [27] L. Oliveira e Silva and J. T. Mendonça, "Kinetic theory of photon acceleration: Time-dependent spectral evolution of ultrashort laser pulses," *Phys. Rev. E, Stat. Phys. Plasmas Fluids Relat. Interdiscip. Top.*, vol. 57, no. 3, pp. 3423–3431, Mar. 1998.
- [28] A. J. W. Reitsma, R. M. G. M. Trines, R. Bingham, R. A. Cairns, J. T. Mendonça, and D. A. Jaroszynski, "Photon kinetic modeling of laser pulse propagation in underdense plasma," *Phys. Plasmas*, vol. 13, no. 11, p. 113 104, Nov. 2006.
- [29] A. J. W. Reitsma, D. A. Jaroszynski, R. M. G. M. Trines, and R. L. Bingham, "Scaling laws for laser–plasma interaction derived with photon kinetic theory," Central Laser Facility, Oxfordshire, U.K. p. 87, "CLF Annual Rep. 2004-2005". [Online]. Available: <http://www.clf.rl.ac.uk/reports/>
- [30] P. Sprangle, J. Krall, and E. Esarey, "Hose-modulation instability of laser pulses in plasmas," *Phys. Rev. Lett.*, vol. 73, no. 26, pp. 3544–3547, Dec. 1994.
- [31] N. E. Andreev, L. M. Gorbunov, V. I. Kirsanov, K. Nakajima, and A. Ogata, "Structure of the wake field in plasma channels," *Phys. Plasmas*, vol. 4, no. 4, pp. 1145–1153, Apr. 1997.
- [32] [Online]. Available: <http://www.epsrc.ac.uk/default.html>



Albert Reitsma received the M.Sc. degree in physics from the University of Utrecht, Utrecht, The Netherlands, and the Ph.D. degree from the Technical University of Eindhoven, Eindhoven, The Netherlands.

He has been with the Department of Physics, University of Strathclyde, Glasgow, since 2002, where his main area of research has been laser–plasma interaction and plasma-based acceleration methods. He was awarded a postdoctoral fellowship in theoretical physics from EPSRC in 2005.



Dino Jaroszynski received the B.S. degree in physics and the Ph.D. degree from the University of Manchester, Manchester, U.K.

After completing his studies, he was a Research Fellow with a number of well-known European laboratories between 1983 and 1996. He is currently with the Department of Physics, University of Strathclyde, Glasgow. His main research activities have been in the area of collective radiation–matter interactions in atomic systems, free-electron laser-like devices, and, more recently, in plasmas. Among

his scientific achievements, the most outstanding was the first demonstration and study of superradiance in a free-electron laser.